Ensemble density functional theory method correctly describes bond dissociation, excited state electron transfer, and double excitations

Michael Filatov,[1,a)] Miquel Huix-Rotllant,[2] and Irene Burghardt[2]
[1]*Department of Chemistry, Southern Methodist University, 3215 Daniel Avenue, Dallas, Texas 75275-0314, USA*
[2]*Institute of Physical and Theoretical Chemistry, Goethe University Frankfurt, Max-von-Laue-Str. 7, D-60438 Frankfurt am Main, Germany*

(Received 19 March 2015; accepted 23 April 2015; published online 11 May 2015)

State-averaged (SA) variants of the spin-restricted ensemble-referenced Kohn-Sham (REKS) method, SA-REKS and state-interaction (SI)-SA-REKS, implement ensemble density functional theory for variationally obtaining excitation energies of molecular systems. In this work, the currently existing version of the SA-REKS method, which included only one excited state into the ensemble averaging, is extended by adding more excited states to the averaged energy functional. A general strategy for extension of the REKS-type methods to larger ensembles of ground and excited states is outlined and implemented in extended versions of the SA-REKS and SI-SA-REKS methods. The newly developed methods are tested in the calculation of several excited states of ground-state multi-reference systems, such as dissociating hydrogen molecule, and excited states of donor–acceptor molecular systems. For hydrogen molecule, the new method correctly reproduces the distance dependence of the lowest excited state energies and describes an avoided crossing between the doubly excited and singly excited states. For bithiophene–perylenediimide stacked complex, the SI-SA-REKS method correctly describes crossing between the locally excited state and the charge transfer excited state and yields vertical excitation energies in good agreement with the *ab initio* wavefunction methods. © *2015 AIP Publishing LLC.* [http://dx.doi.org/10.1063/1.4919773]

I. INTRODUCTION

In density functional theory (DFT),[1,2] the excited states of many-electron fermionic systems are typically accessed through the use of linear-response formalism, as, for example, is implemented in linear-response time-dependent DFT (LR-TD-DFT or TD-DFT, for brevity).[3,4] Although TD-DFT is regarded as a formally exact theory,[5] its practical implementation invokes a number of approximations which often result in large errors for certain types of excited states. In particular, excitations of ground-state multi-reference systems—e.g., molecules with dissociating bonds or weakly coupled magnetic centers—are poorly described by TD-DFT based on the single-determinant Kohn-Sham (KS) method of DFT.[6–8] Charge transfer (CT) excitations, especially long range charge transfer, represent yet another situation where the use of TD-DFT in connection with the commonly adopted adiabatic approximation for the exchange-correlation (XC) kernel leads to very inaccurate predictions.[9,10] There are also other situations where the standardly used TD-DFT methodology fails badly to take proper account of important physical effects thus leading to large errors in the calculated excitation energies.[11,12]

The aforementioned shortcomings of the standard TD-DFT can be remedied by the use of ensemble DFT[13,14] as implemented in the spin-restricted ensemble referenced KS (REKS) method and its state-averaged (SA-REKS) and state-interaction SA-REKS (SI-SA-REKS) variants.[8] Being based on the rigorous formalism of ensemble DFT for excited states,[15] the REKS-type methods furnish a variational approach to obtaining excitation energies,[8,16–18] which has a number of advantages before the response (i.e., perturbational) approach of the standard TD-DFT. In particular, the use of the variational formalism enables one not only to correctly describe excited states of ground-state multi-reference systems (e.g., molecules with dissociating bonds of polyradical species, such as polyacenes[7,8,16]) and real crossings between the ground and excited states,[17,19] the so-called conical intersections, but also to take proper account of the orbital relaxation in the excited state and to accurately describe excitations in systems which represent difficult cases for the standard TD-DFT formalism, such as cyanine dyes and CT transitions in donor–acceptor systems (DA).[7,20]

In this work, a strategy of extending the existing SA-REKS and SI-SA-REKS formalisms to describe more than one excited state of interest is outlined and investigated in practical applications of the method. Bypassing the limitation of the currently existing SA-REKS method to an ensemble of the ground state and only one excited state extends capabilities of the method substantially and allows us to model phenomena such as the excited state electron transfer,[21] in which crossing between the locally excited (LE) state and the CT excited state plays a crucial role. Besides correctly describing excited states

a)Electronic mail: mike.filatov@gmail.com

resulting from one-electron orbital transitions, the extended SI-SA-REKS formalism is capable of correctly describing the double electronic excitations and their mixing with the single excitations; the latter becomes important, e.g., for molecules with dissociating bonds.

The basic features of the REKS-type methods and their extension to include an extra excited state will be described in Sec. II. In Sec. III, the derived extended REKS formalism will be applied to study several systems where real or avoided crossing of the excited states takes place. The studied systems include the excited states of dissociating hydrogen molecule, the LE and CT excited states of 4-(N,N-Dimethyl-amino)benzonitrile (DMABN) chromophore, and the LE and CT excited states of a stacked donor–acceptor complex of bithiophene (BT) and perylenediimide (PD). REKS description of the excited states of these systems will be compared with the results of the standard TD-DFT calculations and with the available *ab initio* wavefunction theory (WFT) results.

II. METHODOLOGY

The REKS and SA-REKS methods[8,16,22,23] utilize ensemble representation of the density and energy[13,24] to describe the non-dynamic electron correlation in the ground and excited states of molecular species.[25,26] The ensemble v-representability (E-VR) property was rigorously proved for an arbitrary fermionic density in seminal works of Lieb[13] and Englisch and Englisch,[14] and the necessity to invoke the ensemble representation to describe strong non-dynamic electron correlation was demonstrated by Schipper *et al.*[25] and by Morrison[26] in a series of first principles Kohn-Sham simulations. Within the ensemble representation of the ground state density, the KS orbitals degenerate at the Fermi level become fractionally occupied[25,27] where their fractional occupation numbers (FON's) can be obtained from stationarity of the energy with respect to FON's variation. As the fractional occupations of the frontier KS orbitals lie beyond the single-determinant representation of the density, commonly employed in the KS method, the energy functionals based on the latter representation cannot be directly used in connection with ensemble densities.[28–30]

A. REKS method for ground states

To make use of ensemble representation of the density and to derive the energy expression suitable for these densities, let us start from the non-interacting reference system. For simplicity, let us focus on a system comprising two frontier KS orbitals containing two electrons in total. As the fractionally occupied orbitals ϕ_r and ϕ_s are degenerate,[25,27] the closed-shell KS determinants $|\cdots\phi_r\bar{\phi}_r\rangle$ and $|\cdots\phi_s\bar{\phi}_s\rangle$ are degenerate as well and the total density is given by a weighted sum

$$\begin{aligned}\rho_s &= \frac{n_r}{2}\rho[\cdots\phi_r\bar{\phi}_r] + \frac{n_s}{2}\rho[\cdots\phi_s\bar{\phi}_s]\\ &= \sum_k n_k|\phi_k|^2 + n_r|\phi_r|^2 + n_s|\phi_s|^2,\end{aligned} \tag{1}$$

where occupation numbers n_k, n_r, and n_s satisfy the condition

$$\begin{gathered} n_k = 2, \quad \varepsilon_k < \mu,\\ 0 \le n_r, n_s \le 2, \quad \varepsilon_r = \varepsilon_s = \mu,\\ \sum_i n_i = N,\end{gathered} \tag{2}$$

and μ is the Fermi level, and ε_i are the respective KS orbital energies, that is, the eigenvalues of the Hamiltonian $\hat{H}^\lambda$ for $\lambda = 0$,[31–33]

$$\hat{H}^\lambda = \sum_i -\frac{1}{2}\nabla_i^2 + \sum_i v_{ext,\lambda}(\vec{r}_i) + \sum_{i>j}\frac{\lambda}{r_{ij}}. \tag{3}$$

In Eq. (3), the external potential $v_{ext,\lambda}(\vec{r})$ depends on the coupling strength λ in such a way that the density ρ_s remains invariant along the adiabatic connection path $0 \le \lambda \le 1$ and $v_{ext,0}(\vec{r}) = v_{KS}(\vec{r})$ is the KS potential and $v_{ext,1}(\vec{r}) = v_{ext}(\vec{r})$ is the physical external potential, e.g., the potential of the nuclei in the molecule.[31,32]

Let us follow the adiabatic connection path starting from $\lambda = 0$ and increase λ infinitesimally, such that only the electrons in the fractionally occupied—hence, degenerate—orbitals are affected by the electron-electron interaction terms in Eq. (3). The energy of the state having density (1) will then be given by the lowest eigenvalue of a secular matrix

$$\begin{pmatrix} E^\lambda[\cdots\phi_r\bar{\phi}_r] & K^\lambda_{rs}\\ K^\lambda_{rs} & E^\lambda[\cdots\phi_s\bar{\phi}_s]\end{pmatrix}, \tag{4}$$

which follows from the application of quasi-degenerate perturbation theory.[34,35] In Eq. (4), $K^\lambda_{rs} = -\frac{1}{2}\big(E^\lambda[\cdots\phi_r\phi_s] - E^\lambda[\cdots\phi_r\bar{\phi}_s] + E^\lambda[\cdots\bar{\phi}_r\bar{\phi}_s] - E^\lambda[\cdots\bar{\phi}_r\phi_s]\big)$ (for $\lambda \to 0$, $K^\lambda_{rs} = \lambda\,(\phi_r\phi_s|\phi_s\phi_r)$) is the coupling element between the configurations $|\cdots\phi_r\bar{\phi}_r\rangle$ and $|\cdots\phi_s\bar{\phi}_s\rangle$ (for small λ, this is the exchange integral between the orbitals ϕ_r and ϕ_s).

Expanding matrix (4) with respect to λ and keeping in the expansion only the term linear in λ, one obtains

$$\begin{aligned}&\begin{pmatrix} E^\lambda[\cdots\phi_r\bar{\phi}_r] & K^\lambda_{rs}\\ K^\lambda_{rs} & E^\lambda[\cdots\phi_s\bar{\phi}_s]\end{pmatrix}\\ &\quad= \begin{pmatrix} E_0[\cdots\phi_r\bar{\phi}_r] & 0\\ 0 & E_0[\cdots\phi_s\bar{\phi}_s]\end{pmatrix} + \lambda\\ &\qquad\times\begin{pmatrix} \dfrac{dE^\lambda[\cdots\phi_r\bar{\phi}_r]}{d\lambda} & \dfrac{dK^\lambda_{rs}}{d\lambda}\\ \dfrac{dK^\lambda_{rs}}{d\lambda} & \dfrac{dE^\lambda[\cdots\phi_s\bar{\phi}_s]}{d\lambda}\end{pmatrix} + O(\lambda^2),\end{aligned} \tag{5}$$

the lowest energy solution of which is given by

$$\begin{aligned}E^\lambda &= \frac{n_r^\lambda}{2}E_0[\cdots\phi_r\bar{\phi}_r] + \frac{n_s^\lambda}{2}E_0[\cdots\phi_s\bar{\phi}_s]\\ &\quad+\lambda\left(\frac{n_r^\lambda}{2}\frac{dE^\lambda[\cdots\phi_r\bar{\phi}_r]}{d\lambda}\right.\\ &\quad\left.+\frac{n_s^\lambda}{2}\frac{dE^\lambda[\cdots\phi_s\bar{\phi}_s]}{d\lambda} - (n_r^\lambda n_s^\lambda)^{1/2}\frac{dK^\lambda_{rs}}{d\lambda}\right).\end{aligned} \tag{6}$$

When deriving Eq. (6), it was used that $E_0[\cdots\phi_r\bar{\phi}_r] = E_0[\cdots\phi_s\bar{\phi}_s]$ and $n_r^\lambda + n_s^\lambda = 2$, and the occupation numbers $n_r^\lambda = 2|c_1^\lambda|^2$ and $n_s^\lambda = 2|c_2^\lambda|^2$ are obtained from the lowest eigenvector $(c_1^\lambda, c_2^\lambda)$ of the matrix in the second line of Eq. (5).[36]

Replacing the occupation numbers n_r^λ and n_s^λ by constant median values, n_r and n_s, assuming that no further degeneracies occur along the adiabatic connection path and performing the coupling constant integration,[31,32] one arrives at

$$\begin{aligned} E_{ens} = &\frac{n_r}{2}E_0[\cdots\phi_r\bar{\phi}_r] + \frac{n_s}{2}E_0[\cdots\phi_s\bar{\phi}_s] \\ &+ \int \rho_s(\mathbf{r})(v_{ext,1}(\mathbf{r}) - v_{ext,0}(\mathbf{r}))d\mathbf{r} \\ &+ \frac{n_r}{2}E_{Hxc}[\cdots\phi_r\bar{\phi}_r] \\ &+ \frac{n_s}{2}E_{Hxc}[\cdots\phi_s\bar{\phi}_s] + \frac{1}{2}(n_r n_s)^{1/2}\Big(E_{Hxc}[\cdots\phi_r\phi_s] \\ &- E_{Hxc}[\cdots\phi_r\bar{\phi}_s] + E_{Hxc}[\cdots\bar{\phi}_r\bar{\phi}_s] - E_{Hxc}[\cdots\bar{\phi}_r\phi_s]\Big), \end{aligned} \tag{7}$$

where the E_{Hxc} terms comprise the Hartree and the XC energy of the given configuration. Substituting the density ρ_s to Eq. (7), noting that the sum of the kinetic energy and the interaction with the external potential $v_{ext,1}$ is the same for all four terms in parentheses in the third line of Eq. (7), one arrives at

$$\begin{aligned} E_{ens} = &\frac{n_r}{2}E_{DFT}[\cdots\phi_r\bar{\phi}_r] + \frac{n_s}{2}E_{DFT}[\cdots\phi_s\bar{\phi}_s] \\ &+ \frac{1}{2}(n_r n_s)^{1/2}\Big(E_{DFT}[\cdots\phi_r\phi_s] - E_{DFT}[\cdots\phi_r\bar{\phi}_s] \\ &+ E_{DFT}[\cdots\bar{\phi}_r\bar{\phi}_s] - E_{DFT}[\cdots\bar{\phi}_r\phi_s]\Big), \end{aligned} \tag{8}$$

which is the main origin of the REKS energy expression.[8,36] In Eq. (8), $E_{DFT}[\cdots\bar{\phi}_p\phi_q]$ is the usual DFT energy of a single-determinant configuration $|\cdots\bar{\phi}_p\phi_q\rangle$. The REKS energy formula

$$\begin{aligned} E^{REKS(2,2)} = &\frac{n_r}{2}E_{DFT}[\cdots\phi_r\bar{\phi}_r] + \frac{n_s}{2}E_{DFT}[\cdots\phi_s\bar{\phi}_s] \\ &+ \frac{1}{2}f(n_r,n_s)\Big(E_{DFT}[\cdots\phi_r\phi_s] - E_{DFT}[\cdots\phi_r\bar{\phi}_s] \\ &+ E_{DFT}[\cdots\bar{\phi}_r\bar{\phi}_s] - E_{DFT}[\cdots\bar{\phi}_r\phi_s]\Big) \end{aligned} \tag{9}$$

was derived from Eq. (8) by interpolating between the strong non-dynamic correlation regime (where Eqs. (1) and (8) are valid) and the weak non-dynamic correlation regime (where a single-determinant representation of the energy and the density is valid) via introducing an interpolating function $f(n_r,n_s)$.[23]

REKS energy formula (9) describes a pair of strongly correlated electrons in two frontier KS orbitals. Energy expressions for other strongly correlated situations (e.g., two electrons in three frontier orbitals) can be derived similarly by applying quasi-degenerate perturbation theory and adiabatic connection integration.[8,36] In the REKS method, energy (9) is minimized with respect to both the KS orbitals and the FON's of the frontier KS orbitals.

B. REKS method for excited states: SA-REKS and SI-SA-REKS

The REKS(2,2) method outlined above describes the ground state of a strongly correlated molecule. Within ensemble DFT,[28] the excited states can be accessed using the formalism developed by Gross, Oliveira, and Kohn[15] (GOK) who proved the variational principle

$$\begin{aligned} \sum_{K=1}^{M}\omega_K\langle\Phi_K|\hat{H}|\Phi_K\rangle \geq \sum_{K=1}^{M}\omega_K E_K, \\ 0 \leq \omega_K \leq 1; \quad \sum_{K=1}^{M}\omega_K = 1, \end{aligned} \tag{10}$$

for ensembles of the ground and several lowest excited states. Thus, considering a two-state ensemble comprising the ground and the lowest excited states and variationally optimizing its energy

$$E_\omega = (1-\omega)E_0 + \omega E_1, \tag{11}$$

one can obtain the excitation energy $\Delta E = E_1 - E_0$ from the ratio in

$$\Delta E = \frac{E_\omega - E_0}{\omega}. \tag{12}$$

Let us use the GOK ensemble formalism[15] in the context of the two-configurational REKS method. For an infinitesimal value of λ in the vicinity of the non-interacting system, the lowest eigenstate of Hamiltonian (3) is given by a two-configurational wavefunction

$$\Phi_0 = \sqrt{\frac{n_r}{2}}\left|\phi_r\bar{\phi}_r\right\rangle - \sqrt{\frac{n_s}{2}}\left|\phi_s\bar{\phi}_s\right\rangle. \tag{13}$$

The lowest singlet excited state is obtained by a one-electron transition which leads to an open-shell singlet (OSS) wavefunction

$$\Phi_1 = \frac{1}{\sqrt{2}}\left|\phi_r\bar{\phi}_s\right\rangle + \frac{1}{\sqrt{2}}\left|\phi_s\bar{\phi}_r\right\rangle. \tag{14}$$

Note that there is also a doubly excited state described by a two-configurational wavefunction

$$\Phi_2 = \sqrt{\frac{n_s}{2}}\left|\phi_r\bar{\phi}_r\right\rangle + \sqrt{\frac{n_r}{2}}\left|\phi_s\bar{\phi}_s\right\rangle, \tag{15}$$

orthogonal to the other two states.[22,20] For the moment however, let us focus on the states Φ_0 and Φ_1.

Let us make a simplifying assumption that the states Φ_0 and Φ_1 are decoupled by symmetry, e.g., as in a homosymmetric diradical. Then, starting from the non-interacting ensemble reference state and performing the coupling strength integration, as was done when deriving the REKS energy formula, the energy of an ensemble of the two states, S_0 and S_1, is described by the SA-REKS method,[16]

$$\begin{aligned} E_\omega^{SA\text{-}REKS} = (1-\omega)E^{REKS(2,2)} + \omega E^{ROKS}, \\ 0 \leq \omega \leq 1, \end{aligned} \tag{16}$$

in which the energy of the S_1 state is described by the spin-restricted open-shell KS (ROKS) method for an OSS state,[37,38]

$$\begin{aligned} E^{ROKS} = &E_{DFT}[\cdots\phi_r\bar{\phi}_s] - \frac{1}{2}E_{DFT}[\cdots\phi_r\phi_s] \\ &+ E_{DFT}[\cdots\bar{\phi}_r\phi_s] - \frac{1}{2}E_{DFT}[\cdots\bar{\phi}_r\bar{\phi}_s]. \end{aligned} \tag{17}$$

Ensemble energy (16) is optimized with respect to the KS orbitals and the FON's of the frontier KS orbitals. Using

the optimized SA-REKS orbitals and FON's, energies of the individual states are calculated by Eqs. (9) and (17) without further orbital optimization.[8,16,36]

So far, the S_0 and S_1 states were assumed decoupled by symmetry. If no symmetry is present or the two states belong in the same irreducible representation, interaction between the states needs to be taken into account. In the vicinity of the non-interacting ensemble reference state, i.e., $\lambda \approx 0$, the decoupled states S_0 and S_1 can be obtained from the eigenvalues of a secular matrix $\begin{pmatrix} E_0^\lambda & \Delta_{01}^\lambda \\ \Delta_{01}^\lambda & E_1^\lambda \end{pmatrix}$, where the off-diagonal matrix element is given by $\Delta_{01}^\lambda = \langle \Phi_0 | \hat{H}^\lambda | \Phi_1 \rangle$.[8,17,18,36] As follows from the application of Slater-Condon rules[39] and open-shell self-consistent field (SCF) formalism,[40] the latter element can be calculated as $\Delta_{01}^\lambda = (\sqrt{n_r^\lambda} - \sqrt{n_s^\lambda})\varepsilon_{rs}^\lambda$, where ε_{rs}^λ is an off-diagonal Lagrange multiplier between the fractionally occupied frontier KS orbitals for the given value of the coupling constant λ.[8,17,18,36] Performing the coupling constant integration,[41] one obtains the decoupled S_0 and S_1 energies as the eigenvalues of the SI-SA-REKS secular matrix

$$\begin{pmatrix} E_0^{REKS} & (\sqrt{n_r} - \sqrt{n_s})\varepsilon_{rs}^{SA\text{-}REKS} \\ (\sqrt{n_r} - \sqrt{n_s})\varepsilon_{rs}^{SA\text{-}REKS} & E_1^{ROKS} \end{pmatrix}, \quad (18)$$

where the E_0^{REKS} and E_1^{ROKS} energies are calculated using the SA-REKS orbitals. The use of the latter orbitals is justified for the ensemble weighting factor $\omega = 1/2$, which is typically employed in the SA-REKS and SI-SA-REKS calculations. The described two-state SI-SA-REKS method can be extended by adding the doubly excited state Φ_2 to secular matrix (18).[20] In this way, the effect of double electronic excitation can be taken into account in the states obtained from a 3×3 secular matrix

$$\begin{pmatrix} E_0^{REKS} & (\sqrt{n_r} - \sqrt{n_s})\varepsilon_{rs}^{SA\text{-}REKS} & 0 \\ (\sqrt{n_r} - \sqrt{n_s})\varepsilon_{rs}^{SA\text{-}REKS} & E_1^{ROKS} & (\sqrt{n_r} + \sqrt{n_s})\varepsilon_{rs}^{SA\text{-}REKS} \\ 0 & (\sqrt{n_r} + \sqrt{n_s})\varepsilon_{rs}^{SA\text{-}REKS} & E_2^{REKS} \end{pmatrix}, \quad (19)$$

where the energy E_2^{REKS} is calculated using the SA-REKS orbitals and the formula

$$\begin{aligned} E_2^{REKS} = {} & \frac{n_s}{2} E_{DFT}[\cdots \phi_r \bar{\phi}_a r] + \frac{n_r}{2} E_{DFT}[\cdots \phi_s \bar{\phi}_s] \\ & - \frac{1}{2} f(n_r, n_s)\Big(E_{DFT}[\cdots \phi_r \phi_s] - E_{DFT}[\cdots \phi_r \bar{\phi}_s] \\ & + E_{DFT}[\cdots \bar{\phi}_r \bar{\phi}_s] - E_{DFT}[\cdots \bar{\phi}_r \phi_s] \Big), \end{aligned} \quad (20)$$

which follows from the second root of secular matrix (4).[20,8,36] The use of the 3-configurational SI-SA-REKS method is beneficial for the description of ground and excited states with charge transfer character, for which the effect of double excitations may become important.[20]

C. Extension of the SA-REKS and SI-SA-REKS methods

So far, the SA-REKS method was designed to tackle two states, the ground state and a single excited state. The excited state is obtained by one-electron transition from the highest occupied molecular orbital (HOMO) to the lowest unoccupied MO (LUMO), i.e., one-electron transition within the REKS active space. If more excited states need to be calculated, the new states need to be included into the ensemble energy. In real situations, often only a handful of excited states need to be calculated to address photophysical and photochemical properties of a wide class of target systems. In this work, an excited state obtained by a single electron transition from the HOMO to the next LUMO (LUMO + 1) will be added to the SA-REKS and SI-SA-REKS energy expressions. In this way, one should be able to describe crossings (real and/or avoided) between the excited states, e.g., relevant for theoretical description of photoinduced charge transfer.

Similar to the derivation of the two-state SA-REKS method, let us make an assumption that the three states, the ground state, the first excited state corresponding to the HOMO → LUMO transition, and the second excited state, the HOMO → LUMO + 1 state, are decoupled, e.g., by symmetry. Then, the latter excited state can be described (in the vicinity of the non-interacting KS reference) by an OSS-type wavefunction

$$\Phi_3 = \frac{1}{\sqrt{2}} \left| \phi_r \bar{\phi}_t \right\rangle + \frac{1}{\sqrt{2}} \left| \phi_t \bar{\phi}_r \right\rangle, \quad (21)$$

where ϕ_t is the LUMO + 1 orbital and its energy can be calculated by the ROKS method as in

$$\begin{aligned} E_3^{ROKS} = {} & E_{DFT}[\cdots \phi_r \bar{\phi}_t] - \frac{1}{2} E_{DFT}[\cdots \phi_r \phi_t] \\ & + E_{DFT}[\cdots \bar{\phi}_r \phi_t] - \frac{1}{2} E_{DFT}[\cdots \bar{\phi}_r \bar{\phi}_t]. \end{aligned} \quad (22)$$

The energy functional of the three-state SA-REKS (3SA-REKS) method is then given by

$$\begin{aligned} E_{\omega_1,\omega_3}^{3SA\text{-}REKS} = {} & (1 - \omega_1 - \omega_3) E_0^{REKS(2,2)} + \omega_1 E_1^{ROKS} \\ & + \omega_3 E_3^{ROKS}; \quad \omega_1, \omega_3 \geq 0; \quad 0 \leq \omega_1 + \omega_3 \leq 1, \end{aligned} \quad (23)$$

and this functional is optimized with respect to the KS orbitals and FON's while keeping the weighting factors ω_1 and ω_3 fixed. In the case when application of the state interaction scheme is deemed necessary, an equiensemble of the three energies is recommended, i.e., $\omega_1 = \omega_3 = 1/3$.

The assumption that the three states in (23) are decoupled by symmetry is often not realistic even for symmetric molecules. Thus, the inclusion of state interaction seems mandatory for obtaining sensible excited states from the state-averaged calculation. Derivation of the SI-SA-REKS method for the case of an extra excited state is similar to the derivation of Eqs. (18) and (19) and leads to diagonalization of the secular matrix

$$\begin{pmatrix} E_0^{REKS} & (\sqrt{n_r}-\sqrt{n_s})\varepsilon_{rs}^{SA\text{-}REKS} & 0 & \sqrt{n_r}\varepsilon_{rt}^{SA\text{-}REKS}-\sqrt{n_s}\Delta_{sr,st} \\ (\sqrt{n_r}-\sqrt{n_s})\varepsilon_{rs}^{SA\text{-}REKS} & E_1^{ROKS} & (\sqrt{n_r}+\sqrt{n_s})\varepsilon_{rs}^{SA\text{-}REKS} & \varepsilon_{st}^{SA\text{-}REKS}+\Delta_{sr,rt} \\ 0 & (\sqrt{n_r}+\sqrt{n_s})\varepsilon_{rs}^{SA\text{-}REKS} & E_2^{REKS} & \sqrt{n_s}\varepsilon_{rt}^{SA\text{-}REKS}+\sqrt{n_r}\Delta_{sr,st} \\ \sqrt{n_r}\varepsilon_{rt}^{SA\text{-}REKS}-\sqrt{n_s}\Delta_{sr,st} & \varepsilon_{st}^{SA\text{-}REKS}+\Delta_{sr,rt} & \sqrt{n_s}\varepsilon_{rt}^{SA\text{-}REKS}+\sqrt{n_r}\Delta_{sr,st} & E_3^{ROKS} \end{pmatrix}, \tag{24}$$

where $\varepsilon_{rt}^{SA\text{-}REKS}$ and $\varepsilon_{st}^{SA\text{-}REKS}$ are the off-diagonal Lagrange multipliers between the respective frontier orbitals in the SA-REKS method, and $\Delta_{sr,st}$ and $\Delta_{sr,rt}$ are calculated (see Appendix for derivation) as in

$$\Delta_{sr,rt} = \frac{1}{2}\left(\langle s|\hat{F}_{r\bar{s}}^{\alpha}|t\rangle - \langle s|\hat{F}_{rs}^{\alpha}|t\rangle - \langle s|\hat{F}_{r\bar{s}}^{\beta}|t\rangle + \langle s|\hat{F}_{rs}^{\beta}|t\rangle\right), \tag{25a}$$

$$\Delta_{sr,st} = \frac{1}{2}\left(\langle r|\hat{F}_{r\bar{s}}^{\alpha}|t\rangle - \langle r|\hat{F}_{rs}^{\alpha}|t\rangle - \langle r|\hat{F}_{r\bar{s}}^{\beta}|t\rangle + \langle r|\hat{F}_{rs}^{\beta}|t\rangle\right), \tag{25b}$$

where $\hat{F}_{r\bar{s}}^{\sigma}$ is the (Kohn-Sham-)Fock operator constructed for the electronic configuration $|\cdots\phi_r\bar{\phi}_s\rangle$ and the spin manifold σ $(=\alpha,\beta)$. The expressions for the off-diagonal elements of secular matrix (24) follow from application of the Slater-Condon rules[39] to the matrix elements $\langle\Phi_0|\hat{H}^{\lambda}|\Phi_3\rangle$, $\langle\Phi_1|\hat{H}^{\lambda}|\Phi_3\rangle$, and $\langle\Phi_2|\hat{H}^{\lambda}|\Phi_3\rangle$, where an infinitesimal coupling strength, $\lambda \approx 0$, is assumed. For $\lambda \approx 0$, the quantities defined in Eq. (25) are given by the respective three-index two-electron integrals, $\Delta_{sr,rt} = \lambda(sr|rt)$ and $\Delta_{sr,st} = \lambda(sr|st)$; however, expressing them via Fock matrix element differences (the Fock operator is a derivative of the energy with respect to a specific orbital, see Appendix) enables one to employ λ-integration for obtaining (25).

Along similar lines, the SA-REKS and SI-SA-REKS methods can be extended further by including more states, e.g., states obtained by the (HOMO − 1 → LUMO) electronic transitions. Noteworthy, mixing between the (HOMO − 1 → LUMO) and (HOMO → LUMO + 1) transitions is important for higher excited states (e.g., S_2) of conjugated aromatic or aliphatic oligomeric molecules, e.g., the ^1L_b state of polyacenes. The inclusion of the (HOMO − 1 → LUMO) transition into the SA-REKS method is straightforward; however, its interaction with the (HOMO → LUMO + 1) transition requires the evaluation of coupling terms which are related to the four-index two-electron integrals of the type $(qs|f_{xc}|rt)$ occurring, e.g., in the **B** matrix of the TD-DFT equations (see Appendix). Although implementation of such an approach does not pose any technical difficulties, in this work, we prefer to focus on the 4SI-3SA-REKS method and to explore its capabilities for describing real and avoided crossings between the excited states relevant, in particular, for photoinduced charge transfer.

III. APPLICATIONS OF EXTENDED SI-SA-REKS METHOD

In this section, the method described above will be applied to a few model systems in which several excited states and their real and avoided crossings will be addressed. The purpose of these applications is not to provide benchmarks of the new method and to flood the reader with MAD numbers (MAD— mean absolute deviation), but to illustrate the range of problems that can be studied with the extended SI-SA-REKS method; the focus will be on qualitative rather than quantitative aspects of the description.

To illustrate the performance of the SI-SA-REKS method and its potential utility, the method will be applied to the dissociating hydrogen molecule, the lowest excited states of DMABN chromophore, and to the excited states of bithiophene perylenediimide stacked DA complex. These model systems cover sufficiently wide range of excited states including single and double excitations of a multi-configurational system (dissociating hydrogen) as well as LE and CT excitations (intramolecular and intermolecular) in DMABN and bithiophene perylenediimide. The SI-SA-REKS results will be compared with the TD-DFT excitation energies as well as with *ab initio* (configuration interaction with single and double excitations (CISD) and second-order approximate coupled cluster (CC2)) excitation energies.

A. Dissociation of hydrogen molecule

Perhaps the simplest system where an avoided crossing of several states takes place is the dissociating hydrogen molecule. Beyond the Coulson-Fischer point (ca. 2.27 bohrs),[42] the ground state electronic configuration $|1\sigma_g 1\bar{\sigma}_g\rangle$ dominating the wavefunction near the equilibrium distance (ca. 1.401 bohrs) undergoes an avoided crossing with the doubly excited electronic configuration $|1\sigma_u 1\bar{\sigma}_u\rangle$ and the ground state of H_2 acquires multi-reference character. Near the same distance, yet another avoided crossing takes place, the crossing between the lowest doubly excited state and the singly excited state dominated by the electronic configuration $\left(|1\sigma_g 2\bar{\sigma}_g\rangle + |2\sigma_g 1\bar{\sigma}_g\rangle\right)/\sqrt{2}$; thus, the $a^1\Sigma_g^+$ state, which was dominated by the latter electronic configuration near the equilibrium distance, becomes a doubly excited state at the elongated H–H distances.

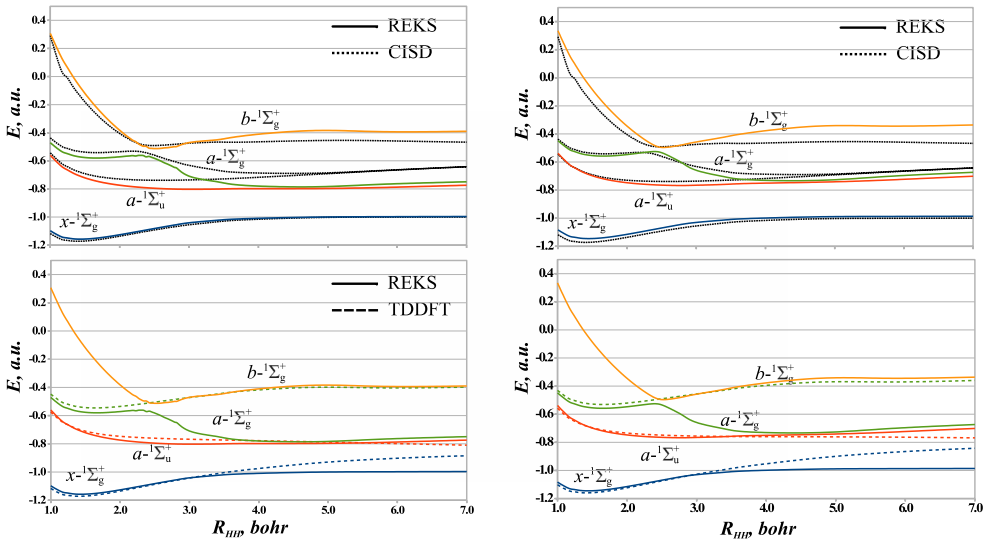

FIG. 1. Potential energy curves of the four lowest singlet states of dissociating H_2 molecule calculated using the 4S3SR-CAM-B3LYP/cc-pVTZ (left panels) and 4S3SR-LC-BLYP/cc-pVTZ (right panels) methods. The upper panels compare the 4S3SR curves with the CISD/cc-pVTZ curves; the lower panels compare the 4S3SR curves with the TD-DFT curves.

The 4SI-3SA-REKS(2,2) method (further abbreviated to 4S3SR) was used in connection with the cc-pVTZ[43] basis set and a number of popular density functionals to describe four lowest singlet states, the ground $x^1\Sigma_g^+$ state, the $a^1\Sigma_u^+$, $a^1\Sigma_g^+$, and $b^1\Sigma_g^+$ excited states, of the dissociating hydrogen molecule. The $1\sigma_g$ and $1\sigma_u$ orbitals were taken to the active space of the REKS(2,2) method and the $2\sigma_g$ orbital was included into the SA-REKS orbital optimization as described in Sec. II. The potential energy curves (PEC's) of these states calculated by the 4S3SR-CAM-B3LYP/cc-pVTZ and 4S3SR-LC-BLYP/cc-pVTZ methods are compared with PEC's obtained using the CISD/cc-pVTZ method and the respective TD-DFT methods.

Generally, both density functionals[44,45] employed in connection with the 4S3SR method describe the PEC's of the four lowest singlet states qualitatively correctly. The 4S3SR-CAM-B3LYP/cc-pVTZ method somewhat underestimates the asymptotic energy of the $a^1\Sigma_u^+$ and $a^1\Sigma_g^+$ states as compared to the CISD/cc-pVTZ curves, while the 4S3SR-LC-BLYP/cc-pVTZ method describes these states more accurately, however somewhat overestimates the asymptotic energy of the $b^1\Sigma_g^+$ state. As seen from comparison of the 4S3SR and TD-DFT PEC's in the lower panels of Figure 1, these features should be attributed to the density functionals employed. Indeed, at long distances, the 4S3SR $b^1\Sigma_g^+$ PEC coincides almost identically with the uppermost TD-DFT PEC for both density functionals. The latter TD-DFT curves represent the singlet excited state dominated by the $\left(|1\sigma_g 2\bar{\sigma}_g\rangle + |2\sigma_g 1\bar{\sigma}_g\rangle\right)/\sqrt{2}$ electronic configuration. As there are no doubly excited states in linear-response adiabatic TD-DFT, the uppermost TD-DFT PEC matches the 4S3SR PEC of the $a^1\Sigma_g^+$ state near the equilibrium distance and the 4S3SR PEC of the $b^1\Sigma_g^+$ state at long H–H distances. At the intermediate distances, the 4S3SR method correctly describes an avoided crossing between the excited states of the Σ_g^+ symmetry which is absent in TD-DFT. Thus, at distances beyond the Coulson-Fischer point, the singly excited Σ_g^+ state and the doubly excited Σ_g^+ state are flipped and the lowest excited state of the Σ_g^+ symmetry becomes a doubly excited state at these distances.

Besides not being capable of capturing double excitations and avoided crossings with the doubly excited states, the standard linear-response adiabatic TD-DFT does not correctly describe PEC of the $a^1\Sigma_u^+$ state at long H–H distances.[6,8,16] Due to the use of the single determinant KS reference state, which is incapable of describing bond dissociation proper way, the standard TD-DFT formalism yields vanishing excitation energy in the dissociation limit of the H–H bond. Although near the equilibrium H–H bond length, TD-DFT PEC of the $a^1\Sigma_u^+$ state is virtually superimposed with the 4S3SR curve, beyond the Coulson-Fisher point, a noticeable deviation from the correct behavior is observed for TD-DFT. The REKS method and its multi-state extensions describe dissociation of the H–H bond correctly and the $a^1\Sigma_u^+$ energy approaches the same asymptote as the energy of the $a^1\Sigma_g^+$ state.[46] It is exactly the picture that is predicted by simple chemical analysis of bond dissociation and confirmed by the results of the CISD calculations. Thus, the 4S3SR method is capable of capturing the most important effects originating due to multi-reference character of the ground and excited states and is capable of delivering accurate results at a mean-field computational cost.

B. Lowest excited states of DMABN

DMABN chromophore displays dual fluorescence where alongside the "normal" fluorescence band (B band), a red-shifted "anomalous" fluorescence band appears in polar solvents.[47] A number of theoretical works have addressed the phenomenon of dual fluorescence whereby it was demonstrated that it is caused by excited state intramolecular CT (ICT) resulting from torsion of the dimethylamino group.[48–51] Along the torsional path, crossing of the two low lying excited states occurs, which leads to changing the character of the lowest excited state from LE to ICT.

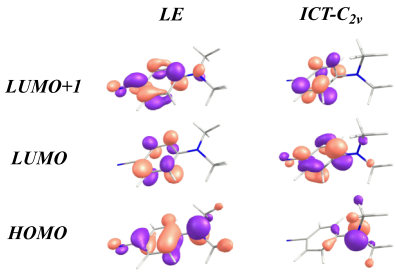

FIG. 2. Frontier orbitals of DMABN obtained using the 4S3SR-CAM-B3LYP/cc-pVTZ method for two conformations along the C_2 symmetric torsional path: the LE minimum and the ICT saddle point (ICT-C_{2v}). See text for more details.

Due to the described features, DMABN is a convenient system to test the newly developed methodology; in particular, its ability to describe crossing between the excited states can be addressed. The lowest excited states of DMABN can be described as almost pure one-electron HOMO → LUMO and HOMO → LUMO + 1 orbital transitions.[51] For nearly coplanar phenyl ring and dimethylamino group, the S_1 state (HOMO → LUMO) has a shallow minimum at ca. 19° of twist and belongs in the *B* symmetry species of the C_2 point group.[51] This state can be characterized as a LE state. Closer to 90° of torsion, the S_1 state acquires a pronounced ICT character and belongs in the *A* symmetry species.[51] Figure 2 shows the frontier orbitals of DMABN obtained using the 4S3SR-CAM-B3LYP/cc-pVTZ method for two conformations along the C_2 symmetric torsion path. The ICT state is further stabilized by pyramidalization distortion of the carbon atom adjacent to the dimethylamino group.[51]

The ability of the 4S3SR method to treat the lowest excited states of DMABN was tested for a number of conformations, the geometries of which were optimized by Köhn *et al.*[51] using the CC2/TZVPP method,[56] as well as for conformations along the C_2 symmetric dimethylamino group torsion path. Table I reports the vertical excitation energies of DMABN obtained using the 4S3SR, TD-DFT, and CC2 methods in connection with the cc-pVTZ basis set[43] for the four conformations from Köhn and Hättig.[51] The latter conformations include the ground state minimum, S_0^{min}, a minimum corresponding to the LE state, $S_1^{LE,min}$, a C_{2v} symmetric saddle point on the ICT excited state PES corresponding to 90° twist of the dimethylamino group, $S_1^{ICT-C_{2v},TS}$, and the ICT excited state minimum, $S_1^{ICT,min}$. In Figure 3 the calculated vertical excitation energies are presented in graphics form.

For all the conformations reported in Table I and Figure 3, there is a noticeable dependence of the TD-DFT vertical excitation energy on the functional employed. The hybrid functionals with a greater fraction of the Fock exchange (BH&HLYP)[54] or range separated hybrids (CAM-B3LYP[45] and LC-BLYP[44]) yield the excitation energies closer to the CC2 values than the functionals with less (B3LYP)[53] or no Fock exchange (BLYP).[52] For ICT conformations (right panels of Figure 3), the latter functionals strongly underestimate the excitation energies, in accord with general experience with these functionals. For the same conformations however, the 4S3SR method yields more stable results in sufficiently uniform agreement with the CC2 reference values even when B3LYP and BLYP functionals are employed.

As was observed previously by Ziegler *et al.*,[57,58] an insufficient orbital relaxation in the excited state is often the cause of unsatisfactory description of the CT transitions by linear response adiabatic TD-DFT formalism. A similar observation was also made in Ref. 20, where the SI-SA-REKS (SSR) method was employed to describe CT excitations. As the 4S3SR method optimizes orbitals variationally for the ground and for the excited states, thus fully accounting for the orbital relaxation effects due to the CT transition, the calculated CT vertical transition energies display less sensitivity to the peculiarities of the functional employed. For LE excitations however, where the orbital relaxation effects are less significant, the functional employed in connection with the 4S3SR method matters as much as for TD-DFT. For LE conformations (left panels of Figure 3), both methods, 4S3SR and TD-DFT, yield similar trends in the excitation energies, where the functionals with large fraction of Fock

TABLE I. Energies (eV) of the lowest vertical transitions of DMABN.

				BLYP[52]		B3LYP[53]		BH&HLYP[54]		CAM-B3LYP[45]		LC-BLYP[44]	
Conformation[a]	State	Experiment[b]	CC2[c]	4S3SR	TD	4S3SR	TD	4S3SR	TD	4S3SR	TD	4S3SR	TD
$S_0^{min,d}$	S_1	4.25	4.44	3.84	4.02	4.28	4.42	4.93	4.90	4.76	4.69	5.27	4.92
	S_2	4.56	4.80	4.05	4.31	4.54	4.65	5.18	4.99	5.00	4.90	5.34	5.08
$S_1^{LE,min,e}$	S_1	3.76	3.80	3.55	3.40	3.90	3.80	4.38	4.32	4.24	4.11	4.56	4.37
	S_2		4.57	3.61	4.12	4.12	4.48	4.80	4.86	4.63	4.76	5.05	4.96
$S_1^{ICT,min,f}$	S_1	2.80	2.50	2.49	1.43	2.54	2.06	2.32	3.02	2.45	2.64	2.36	3.19
	S_2		4.11	4.04	2.98	4.29	3.74	4.30	4.75	4.31	4.50	4.33	4.89
$S_1^{ICT-C_{2v},TS,g}$	S_1		3.29	3.12	1.87	3.44	2.67	3.03	3.81	3.07	3.39	3.08	4.04
	S_2		4.88	4.22	2.80	4.54	3.71	4.32	5.09	4.31	4.59	4.38	5.21

[a]The CC2 optimized geometries are taken from Ref. 51.
[b]Experimental energies of vertical transitions from Refs. 51 and 55.
[c]CC2 energies of vertical transitions calculated in this work.
[d]Ground state equilibrium geometry.
[e]Excited state minimum corresponding to LE.
[f]Excited state minimum corresponding to ICT.
[g]Excited state saddle point (C_{2v}-symmetric transition state) corresponding to ICT.

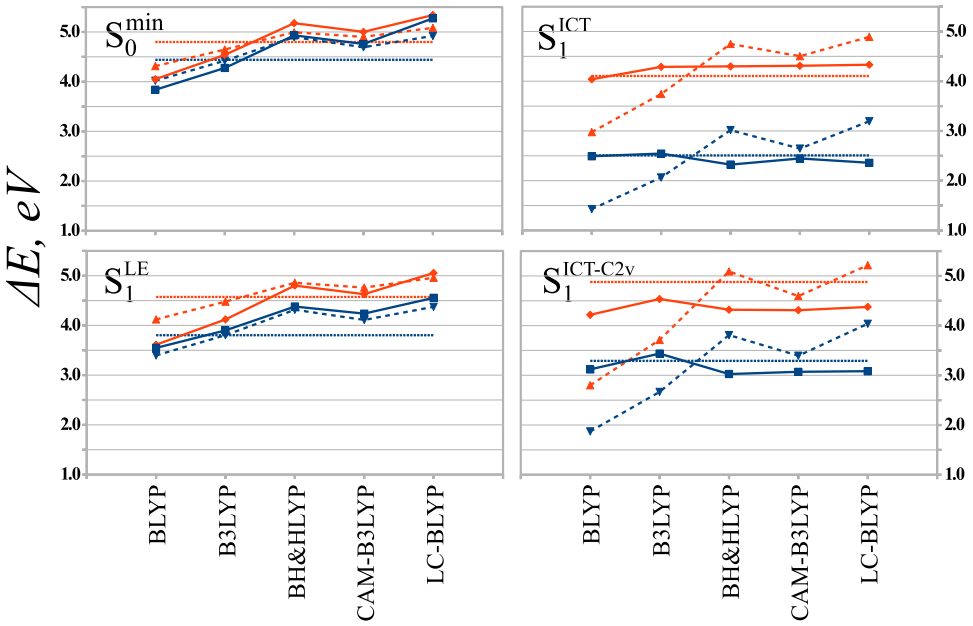

FIG. 3. Energies (eV) of the lowest vertical transitions (blue: $S_1 \leftarrow S_0$, red: $S_2 \leftarrow S_0$) of DMABN calculated using various density functionals in comparison with the CC2 excitation energies. The solid lines represent the 4S3SR results, the dashed lines—the TD results and the dotted lines—the CC2 results. The vertical transitions are calculated for the following conformations: the ground state equilibrium geometry (S_0^{min}), the LE excited state minimum (S_1^{LE}), the ICT excited state minimum (S_1^{ICT}), and the C_{2v}-symmetric ICT excited transition state ($S_1^{ICT-C_{2v}}$). The geometries of these conformations were taken from Ref. 51.

exchange or range separated hybrids yield results in closer agreement with the target CC2 values. There is also a sufficiently close match between the 4S3SR and TD-DFT excitation energies.

The proximity of the 4S3SR and TD-DFT excitation energies is further illustrated by Figure 4, where the profiles of the S_1 and S_2 PES's are shown along the dimethylamino group torsional path. The geometries of conformations along this path were optimized for the lowest excited state using the CC2/cc-pVTZ method by constraining the torsional angle Θ and relaxing all other geometric parameters under the C_2 symmetry. As seen in Figure 4, both methods, 4S3SR and TD-DFT, sufficiently closely reproduce the shape of the excited states PES's and yield crossing between the states of *A* and *B* symmetry in close proximity to the CC2 results. These comparisons indicate that the proposed 4S3SR methodology is a reliable tool for investigating the excited state PES's, which, in addition to the standard TD-DFT, enables one to accurately study excitations of multi-reference systems and charge transfer excitations.

C. Charge transfer and local excitations in bithiophene perylenediimide dimers

Excited state electron transfer in donor–acceptor (DA) systems is a central event in photovoltaic and photosynthetic systems.[21] As the synthetic or biological DA systems are sufficiently large, the first principles wavefunction methods cannot be routinely applied to study their excited states, and DFT/TD-DFT methods are typically used instead. TD-DFT however experiences certain difficulties with the accurate description of CT excited states[9,10] and the use of range separated XC functionals or functionals specifically tuned for this type of excitations is generally recommended.[10]

Here, we apply the 4S3SR formalism to study the lowest excited states, both LE and CT, of stacked bithiophene–perylenediimide dimer as a representative DA system. PD offers a potential replacement for fullerene as an acceptor in organic photovoltaic devices[59] and a number of theoretical investigations of PD-based compounds were already published.[60]

The geometry of the stacked BT–PD complex was optimized previously for the LE state using the CC2 method with def-SV(P) basis set.[61] As we would like to inspect qualitatively the ability of the 4S3SR method to describe the LE and intermolecular CT excited states, the use of geometry optimized with another method appears acceptable and we did not attempt to re-optimize the geometry for each density functional employed in this work.

Let us first inspect the dependence of the LE and CT excited state energies on the interplanar distance in the face-to-face stacked BT–PD dimer. Figure 5 shows the S_0, S_1, and S_2 energy profiles along the interplanar distance R_{bp} (see also the inset in Figure 5) obtained using the ωB97XD density functional[62] in connection with the cc-pVDZ basis set.[43] The ωB97XD functional includes an empirical dispersion correction which is important for obtaining reasonable interfragment interaction in stacked complexes.[62] At longer interplanar distances (R_{bp} > 5 Å), both methods, 4S3SR and TD-DFT, predict the S_1 state to be a LE state, whereas the S_2 state is a CT state. At the TD-DFT level, both states correspond to almost pure HOMO → LUMO + 1 (S_1) and HOMO → LUMO (S_2) orbital transitions.

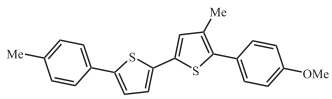

Bithiophene (BT):
5-(4-methoxyphenyl)-4-methyl-5-(4-methylphenyl)-2,2-bithiophene

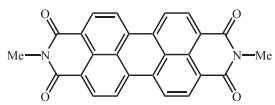

Perylenediimide (PD):
N,N-dimethylperylene-3,4,9,10-dicarboximide

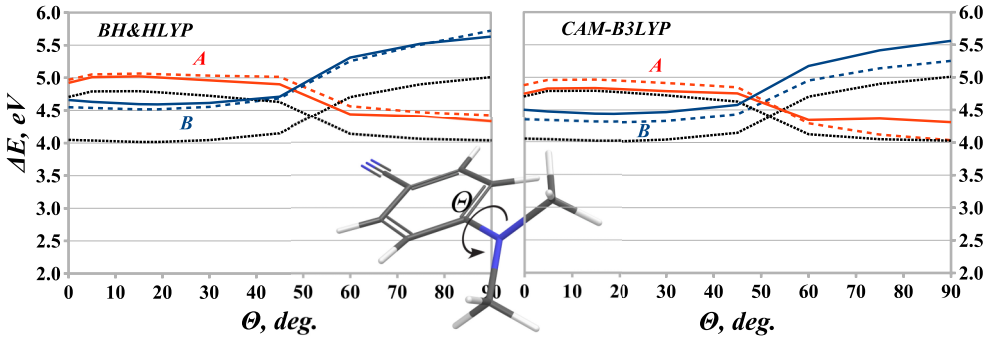

FIG. 4. The energy profiles (eV) of the two lowest excited states of DMABN as a function of the torsion angle Θ (deg) along the C_2 symmetric torsion pathway. The energies are given relative to the ground state planar conformation (Θ = 0). The states are labeled by their symmetry species, A (red) and B (blue), in the C_2 point group. The geometries along the pathway are optimized for the lowest excited state using the CC2/cc-pVTZ method. The black dotted curves show the CC2 energies, the colored dashed curves—the TD-DFT energies, and the solid colored curves—the 4S3SR energies. The DFT calculations are carried out using the BHHLYP (left panel) and CAM-B3LYP (right panel) density functionals.

At shorter R_{bp} distances, the S_1 and S_2 states obtained by 4S3SR and TD-DFT show different nature: At the 4S3SR level, the CT and LE states undergo an avoided crossing near $R_{bp} \approx 4.8$ Å and the CT state becomes the lowest excited state at shorter distances. At the TD-DFT level however, the S_1 state remains LE and no crossing between the LE and CT is observed. At an intermediate distance $R_{bp} = 4.38$ Å, the lowest excited states were also obtained at the CC2/cc-pVDZ level and the S_1 state is a CT state while S_2 is LE.[63] This is the same state ordering as predicted by 4S3SR, but not by TD-DFT. Surprisingly, TD-ωB97XD was unable to describe the excited state crossing which is the key to modeling excited state charge transfer.

The CT and LE vertical excitation energies at the BT–PD distance $R_{bp} = 4.38$ Å calculated using 4S3SR and TD-DFT with a variety of functionals are compared in Table II with the CC2/cc-pVDZ energies. As seen in Table II, the 4S3SR method systematically predicts the CT state below the LE state and the energy splitting between the two states remains almost independent of the functional employed. As can be judged from the CC2/cc-pVDZ results, this is the correct state ordering at this R_{bp}. TD-DFT with long-range corrected functionals puts the CT state above the LE state and, as seen in Figure 5, this state ordering persists over the whole range of R_{bp} distances. Furthermore, the splitting between the CT and LE states is strongly dependent on the functional employed in the context of TD-DFT. Surprisingly, the BH&HLYP functional predicts very close vertical excitation energies and the same state ordering when used in connection with both theoretical methods, 4S3SR and

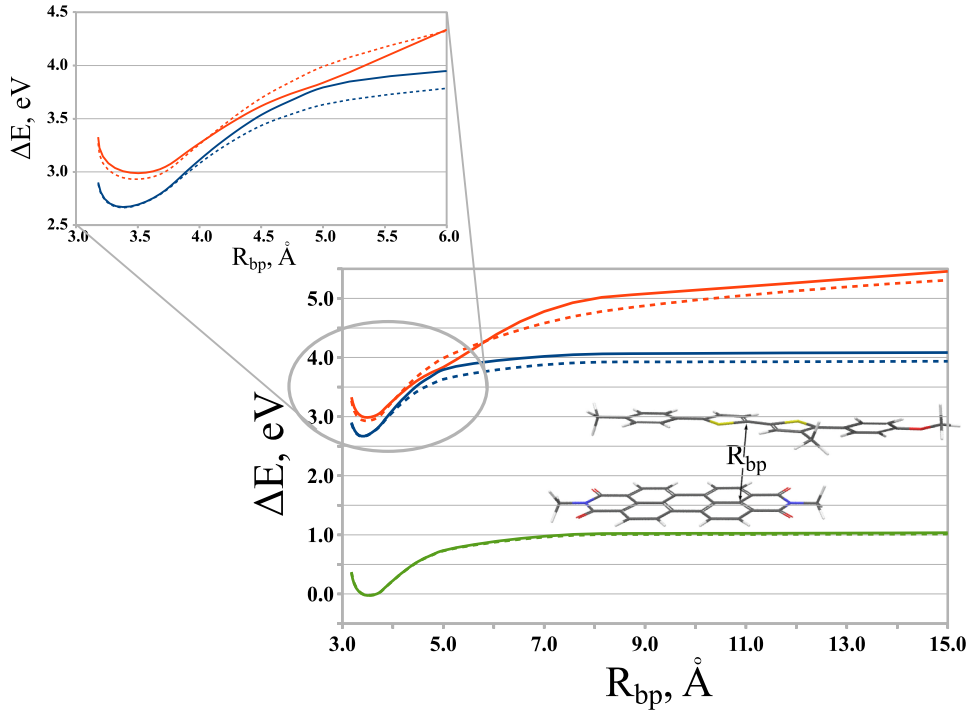

FIG. 5. Energy profiles (in eV) of S_0 (green), S_1 (blue), and S_2 (red) states of stacked bithiophene–perylenediimide dimer along the interplanar distance coordinate R_{bp}. Solid lines—4S3SR and dashed lines—TD-DFT. All the calculations employ ωB97XD functional in connection with the cc-pVDZ basis set. For each method, the energies are given with respect to the lowest S_0 energy.

TABLE II. Vertical excitation energies (eV) of the lowest CT and LE transitions of the BP–PD complex at the interplanar distance $R_{bp} = 4.38$ Å. The lowest excited state is given boldface.

	CT		LE	
Method	4S3SR	TD	4S3SR	TD
BLYP	**1.69**	**0.96**	1.78	2.42
B3LYP	**2.11**	**1.62**	2.19	2.54
BH&HLYP	**2.74**	**2.66**	2.81	2.83
CAM-B3LYP	**2.81**	2.88	2.89	**2.81**
ωB97XD	**2.97**	3.12	3.06	**2.89**
LC-BLYP	**3.47**	4.13	3.58	**3.04**
CC2	**2.79**		3.10	

TD-DFT. However, the more reliable long-range corrected functionals, especially those equipped with the empirical dispersion correction, such as ωB97XD, yield the correct state ordering and reliable excitation energies only when applied in connection with the 4S3SR method. Hence, the latter method can be employed as a reliable computational tool for studying excited state electron transfer.

IV. CONCLUSIONS

In this work, we explored a strategy for extending the SA-REKS and SI-SA-REKS methods[8,16–18,36] to describe several excited states of interest. The SA-REKS and SI-SA-REKS methods, which are based on ensemble DFT for excited states,[15] were initially derived to include one excited state alongside the ground electronic state into the ensemble averaging.[16] Although the two-state variant of the (SI-)SA-REKS method optimizes both states variationally (through the application of the GOK ensemble variational principle)[15] and, therefore, correctly describes their real and avoided crossings,[8,17,19] the limitation to only one excited state restricted applicability of the method and narrowed down the range of problems which could be tackled using this approach.

Here, we investigated a possibility to extend the number of excited states treated variationally by the (SI-)SA-REKS method by including into the ensemble averaging more OSS-type electronic configurations generated by one-electron orbital transitions beyond the REKS active space (usually, the HOMO–LUMO space). As a first step, a three-state SA-REKS formalism, where a HOMO → LUMO + 1 transition was added to the ground and the HOMO → LUMO excited states, was implemented and tested. The individual states, the averaged energy of which is given by the 3SA-REKS functional, are decoupled in the state interaction procedure; a HOMO → LUMO doubly excited state can be added to the latter thus leading to the 4SI-3SA-REKS method.

The developed 4SI-3SA-REKS method was tested in the calculation of lowest excited states of several model systems ranging from the simplest (H_2 molecule) to more complicated molecules (DMABN) and molecular complexes (bithiophene–perylenediimide). For hydrogen molecule, the 4SI-3SA-REKS method was capable to accurately describe the avoided crossing between the $a^1\Sigma_g^+$ and $b^1\Sigma_g^+$ states due to the involvement of double electronic excitation, which is entirely missing in the TD-DFT description.

The ability of the 4SI-3SA-REKS method to describe crossing between the locally excited and charge transfer excited states is documented in the study of DMABN and bithiophene–perylenediimide complex. For the latter complex, the 4SI-3SA-REKS method yields the correct ordering of the LE and CT excited states, which is confirmed by comparison with the CC2 calculations, whereas the TD-DFT predictions strongly depend on the density functional employed. Furthermore, using a popular ωB97XD functional,[62] the 4SI-3SA-REKS method correctly describes an avoided crossing between the LE and CT excited states in this complex, whereas no such crossing is observed in the TD-DFT calculation. Hence, the extended SI-SA-REKS methodology furnishes a versatile computational tool capable of accurately describing situations beyond the current reach of the linear-response TD-DFT approach.

Importantly, in the 4SI-3SA-REKS method, the coupling matrix elements in the secular matrix are expressed entirely in terms of DFT quantities and no two-electron integrals from *ab initio* WFT are used. In particular, the coupling matrix elements between the OSS-type configurations, which at the WFT level involve the three-index two-electron integrals, were obtained as the first derivatives of the single-determinant KS energies with respect to the KS orbitals (in other words, differences between the respective off-diagonal Fock matrix elements). It was also demonstrated that the coupling matrix elements, which at the WFT level are expressed through the four-index two-electron integrals, can be obtained as the second derivatives of the respective single-determinant KS energies with respect to the KS orbitals. Thus, a complete state-interaction secular matrix can be built for any number of states included into the state averaging by using DFT energies and their derivatives only. The successful implementation of the 4SI-3SA-REKS method paves a way to extend the formalism even further and to describe more excited states, a goal that will be pursued in the future work.

ACKNOWLEDGMENTS

M.H.-R. thanks the Alexander von Humboldt Foundation for a postdoctoral fellowship.

APPENDIX: DERIVATION OF EQ. (25)

Let us assume that we would like to describe coupling between the configuration state functions (CSF's) Φ_0 (13) and Φ_3 (21) for Hamiltonian (3) with $\lambda \approx 0$. Applying Slater-Condon rules, one obtains

$$\begin{aligned}\langle\Phi_0|\hat{H}^\lambda|\Phi_3\rangle &= \frac{\sqrt{n_r}}{2}\langle\bar{\phi}_r|\hat{F}_t^\lambda|\bar{\phi}_t\rangle + \frac{\sqrt{n_r}}{2}\langle\phi_r|\hat{F}_t^\lambda|\phi_t\rangle \\ &\quad - \lambda\frac{\sqrt{n_s}}{2}\langle\phi_s\bar{\phi}_s|\phi_r\bar{\phi}_t\rangle - \lambda\frac{\sqrt{n_s}}{2}\langle\phi_s\bar{\phi}_s|\phi_t\bar{\phi}_r\rangle \\ &= \sqrt{n_r}\varepsilon_{rt}^\lambda - \lambda\sqrt{n_s}\,(\phi_s\phi_r|\phi_s\phi_t)\,, \qquad \text{(A1)}\end{aligned}$$

where $\hat{F}_t^\lambda$ is the Fock operator for the orbital ϕ_t and the coupling strength λ, ε_{rt}^λ is a shorthand notation for the

respective off-diagonal matrix element (Lagrange multiplier), both the Dirac notation $\langle\cdots|\cdots\rangle$ and the Mulliken notation $(\cdots|\cdots)$ are used for the two-electron integrals.

Let us further assume that there are no core electrons in the electronic configurations described by CSF's Φ_0 and Φ_3; the presence or absence of the core electrons does not make any difference, as their contributions should cancel out in the final expressions; however, their absence simplifies the respective derivations. To remind the reader that the Fock operator for a single-determinant electronic configuration with n_α α-spin electrons and n_β β-spin electrons is given by

$$\hat{F}^\alpha = \hat{h} + \sum_p^{n_\alpha} \left(\hat{J}_p^\alpha - \hat{K}_p^\alpha\right) + \sum_q^{n_\beta} \hat{J}_q^\beta, \tag{A2}$$

$$\hat{F}^\beta = \hat{h} + \sum_q^{n_\beta} \left(\hat{J}_q^\beta - \hat{K}_q^\beta\right) + \sum_p^{n_\alpha} \hat{J}_q^\alpha, \tag{A3}$$

where the Coulomb $\hat{J}_q^\sigma$ and exchange $\hat{K}_q^\sigma$ operators are defined in the usual way.

Writing down a Fock matrix elements $\langle\phi_r|\hat{F}_{r\bar{s}}^{\sigma,\lambda}|\phi_t\rangle$ for the electronic configuration $|\phi_r\bar{\phi}_s\rangle$, one obtains (due to orbital orthogonality $h_{rt} = 0$)

$$\begin{aligned}\langle\phi_r|\hat{F}_{r\bar{s}}^{\alpha,\lambda}|\phi_t\rangle &= \lambda\,(\phi_r\phi_t|\phi_r\phi_r) - \lambda\,(\phi_r\phi_r|\phi_t\phi_r)\\ &\quad + \lambda\,(\phi_r\phi_t|\phi_s\phi_s)\,,\end{aligned} \tag{A4}$$

$$\begin{aligned}\langle\phi_r|\hat{F}_{r\bar{s}}^{\beta,\lambda}|\phi_t\rangle &= \lambda\,(\phi_r\phi_t|\phi_s\phi_s) - \lambda\,(\phi_r\phi_s|\phi_t\phi_s)\\ &\quad + \lambda\,(\phi_r\phi_t|\phi_r\phi_r)\,.\end{aligned} \tag{A5}$$

For the electronic configuration $|\phi_r\phi_s\rangle$, the respective Fock matrix elements are given by

$$\begin{aligned}\langle\phi_r|\hat{F}_{rs}^{\alpha,\lambda}|\phi_t\rangle &= \lambda\,(\phi_r\phi_t|\phi_r\phi_r) - \lambda\,(\phi_r\phi_r|\phi_t\phi_r)\\ &\quad + \lambda\,(\phi_r\phi_t|\phi_s\phi_s) - \lambda\,(\phi_r\phi_s|\phi_t\phi_s)\,,\end{aligned} \tag{A6}$$

$$\langle\phi_r|\hat{F}_{rs}^{\beta,\lambda}|\phi_t\rangle = \lambda\,(\phi_r\phi_t|\phi_r\phi_r) + \lambda\,(\phi_r\phi_t|\phi_s\phi_s)\,. \tag{A7}$$

Combining the above equations, one obtains the two-electron integral $\lambda\,(\phi_s\phi_r|\phi_s\phi_t)$ as

$$\begin{aligned}\lambda\,(\phi_s\phi_r|\phi_s\phi_t) = \frac{1}{2}\Big(&\langle\phi_r|\hat{F}_{r\bar{s}}^{\alpha,\lambda}|\phi_t\rangle - \langle\phi_r|\hat{F}_{rs}^{\alpha,\lambda}|\phi_t\rangle\\ &- \langle\phi_r|\hat{F}_{r\bar{s}}^{\beta,\lambda}|\phi_t\rangle + \langle\phi_r|\hat{F}_{rs}^{\beta,\lambda}|\phi_t\rangle\Big).\end{aligned} \tag{A8}$$

The Fock operator originates from derivative of the total electronic energy of the given (single-determinant) configuration with respect to a specific orbital,

$$\hat{F}^\sigma\phi_p^\sigma = \frac{\partial E(n_\alpha, n_\beta)}{\partial\phi_p^{\sigma*}}, \tag{A9}$$

and a complex conjugate expression. Hence, Eq. (A8) can be rewritten as

$$\begin{aligned}\lambda\,(\phi_s\phi_r|\phi_s\phi_t) = \frac{1}{2}\Big(&\langle\frac{\partial E_{r\bar{s}}^\lambda}{\partial\phi_r}|\phi_t\rangle - \langle\frac{\partial E_{rs}^\lambda}{\partial\phi_r}|\phi_t\rangle\\ &- \langle\frac{\partial E_{r\bar{s}}^\lambda}{\partial\bar{\phi}_r}|\bar{\phi}_t\rangle + \langle\frac{\partial E_{rs}^\lambda}{\partial\bar{\phi}_r}|\bar{\phi}_t\rangle\Big),\end{aligned} \tag{A10}$$

where the corresponding two-electron three-index integral is given in terms of energy derivatives only. As the density and the KS orbitals remain invariant along the λ-integration path, the coupling strength integration of the energies in Eq. (A10) can be carried out and this leads to Eq. (25) in the main text.

Differentiating energy differences occurring in Eq. (A10) twice with respect to the KS orbitals yields four-index two-electron integrals which are occurring when describing coupling between the CSF's $\frac{1}{\sqrt{2}}|\phi_q\bar{\phi}_s\rangle + \frac{1}{\sqrt{2}}|\phi_s\bar{\phi}_q\rangle$ and $\frac{1}{\sqrt{2}}|\phi_r\bar{\phi}_t\rangle + \frac{1}{\sqrt{2}}|\phi_t\bar{\phi}_r\rangle$. The latter electronic configurations may, for example, be obtained by (HOMO − 1) → LUMO and HOMO → (LUMO + 1) one-electron transitions. Thus, differentiation of the energy difference $E_{r\bar{s}}^\lambda - E_{rs}^\lambda$ with respect to the orbitals ϕ_r and $\bar{\phi}_s$ yields

$$\frac{1}{2}\left\langle\frac{\partial^2}{\partial\bar{\phi}_s\partial\phi_r}\left(E_{r\bar{s}}^\lambda - E_{rs}^\lambda\right)|\phi_t\bar{\phi}_q\right\rangle = \lambda\left(\phi_r\phi_t|\phi_s\phi_q\right), \tag{A11}$$

which can be λ-integrated to yield the required coupling term as the second derivative of the differences of energies of single KS determinants. As flipping the spins of all electrons in Eqs. (A10) and (A11) does not affect the final result, these equations can be symmetrized.

[1]P. Hohenberg and W. Kohn, Phys. Rev. **136**, B864 (1964).
[2]W. Kohn and L. J. Sham, Phys. Rev. **140**, A1133 (1965).
[3]M. E. Casida, C. Jamorski, F. Bohr, J. G. Guan, and D. R. Salahub, *Symposium on Nonlinear Optical Materials—Theory and Modeling, at the 208th National Meeting of the American-Chemical-Society, Washington, DC, August 21–25, 1994. Nonlinear Optical Materials: Theory and Modeling*, ACS Symposium Series Vol. 628, edited by S. P. Karna and A. T. Yeates (American Chemical Society, 1996), pp. 145–163.
[4]M. E. Casida and M. Huix-Rotllant, Annu. Rev. Phys. Chem. **63**, 287 (2012).
[5]M. A. L. Marques and E. K. U. Gross, *A Primer in Density-Functional Theory*, Lecture Notes in Physics Vol. 620, edited by C. Fiolhais, F. Nogueira, and M. A. L. Marques, (Springer, Berlin, 2003), pp. 144–184.
[6]F. Aryasetiawan, O. Gunnarsson, and A. Rubio, Europhys. Lett. **57**, 683 (2002).
[7]M. Filatov and M. Huix-Rotllant, J. Chem. Phys. **141**, 024112 (2014).
[8]M. Filatov, WIREs: Comput. Mol. Sci. **5**, 146 (2015).
[9]A. Dreuw, J. L. Weisman, and M. Head-Gordon, J. Chem. Phys. **119**, 2943 (2003).
[10]T. Stein, L. Kronik, and R. Baer, J. Am. Chem. Soc. **131**, 2818 (2009).
[11]N. T. Maitra, F. Zhang, R. Cave, and K. Burke, J. Chem. Phys. **120**, 5932 (2004).
[12]B. G. Levine, C. Ko, J. Quenneville, and T. J. Martínez, Mol. Phys. **104**, 1039 (2006).
[13]E. H. Lieb, Int. J. Quantum Chem. **24**, 243 (1983).
[14]H. Englisch and R. Englisch, Phys. Status Solidi B **123**, 711 (1984); **124**, 373 (1984).
[15]E. K. U. Gross, L. N. Oliveira, and W. Kohn, Phys. Rev. A **37**, 2805 (1988); **37**, 2809 (1988); L. N. Oliveira, E. K. U. Gross, and W. Kohn, *ibid.* **37**, 2821 (1988).
[16]A. Kazaryan, J. Heuver, and M. Filatov, J. Phys. Chem. A **112**, 12980 (2008).
[17]M. Filatov, J. Chem. Theory Comput. **9**, 4526 (2013).
[18]M. Huix-Rotllant, M. Filatov, S. Gozem, I. Schapiro, M. Olivucci, and N. Ferré, J. Chem. Theory Comput. **9**, 3917 (2013).
[19]A. Nikiforov, J. A. Gamez, W. Thiel, M. Huix-Rotllant, and M. Filatov, J. Chem. Phys. **141**, 124122 (2014).
[20]M. Filatov, J. Chem. Phys. **141**, 124123 (2014).
[21]G. J. Kavarnos, *Fundamentals of Photoinduced Electron Transfer* (Wiley-VCH Verlag GmbH, New York, 1993).
[22]M. Filatov and S. Shaik, Chem. Phys. Lett. **304**, 429 (1999).
[23]I. d. P. R. Moreira, R. Costa, M. Filatov, and F. Illas, J. Chem. Theory Comput. **3**, 764 (2007).
[24]B. Farid, J. Phys.: Condens. Matter **10**, L1 (1998).
[25]P. R. T. Schipper, O. V. Gritsenko, and E.-J. Baerends, Theor. Chem. Acc. **99**, 329 (1998); J. Chem. Phys. **111**, 4056 (1999).
[26]R. C. Morrison, J. Chem. Phys. **117**, 10506 (2002).
[27]K. J. H. Giesbertz and E.-J. Baerends, J. Chem. Phys. **132**, 194108 (2010).
[28]L. N. Oliveira, E. K. U. Gross, and W. Kohn, Int. J. Quantum Chem., Quantum Chem. Symp. **38** (Supp. 24), 707 (1990).
[29]N. I. Gidopoulos, P. G. Papaconstantinou, and E. K. U. Gross, Phys. Rev. Lett. **88**, 033003 (2002).
[30]E. Pastorczak and K. Pernal, J. Chem. Phys. **140**, 18A514 (2014).

[31]P. Noziéres and D. Pines, *The Theory of Quantum Liquids* (Perseus Books Publishing LLC, Cambridge, MA, 1966), pp. 296–298.
[32]A. D. Becke, J. Chem. Phys. **88**, 1053 (1988).
[33]O. Franck and E. Fromager, Mol. Phys. **112**, 1684 (2014).
[34]J. H. Van Vleck, Phys. Rev. **33**, 467 (1929).
[35]P. Löwdin, J. Chem. Phys. **19**, 1396 (1951).
[36]M. Filatov, in *Density Functional Theory of Excited States*, Topics in Current Chemistry, edited by N. Ferré, M. Filatov, and M. Huix-Rotllant (Springer, Berlin, 2015).
[37]T. Ziegler, A. Rauk, and E. J. Baerends, Theor. Chim. Acta **43**, 261 (1977).
[38]M. Filatov and S. Shaik, Chem. Phys. Lett. **288**, 689 (1998).
[39]J. C. Slater, Phys. Rev. **34**, 1293 (1929); E. U. Condon, *ibid.* **36**, 1121 (1930).
[40]K. Hirao and H. Nakatsuji, J. Chem. Phys. **59**, 1457 (1973).
[41]As the density remains invariant along the λ-integration path, the integration does not mix the states Φ_0 and Φ_1. Otherwise, as these states are connected by one-electron transition, the density would not remain invariant.
[42]C. A. Coulson and I. Fischer, Philos. Mag. **40**, 386 (1949).
[43]T. H. Dunning, Jr., J. Chem. Phys. **90**, 1007 (1989).
[44]H. Iikura, T. Tsuneda, T. Yanai, and K. Hirao, J. Chem. Phys. **115**, 3540 (2001).
[45]T. Yanai, D. Tew, and N. C. Handy, Chem. Phys. Lett. **393**, 51 (2004).
[46]As seen in Figure 1, the $a^1\Sigma_g^+$ and $a^1\Sigma_u^+$ curves obtained using the LC-BLYP and CAM-B3LYP XC functionals develop a small gap at long internuclear separations. The gap is caused by the self-interaction error of the approximate XC functionals which leads to a certain error in the 3-index two-electron integrals estimated by Eq. (25). The gap completely disappears, if a self-interaction-free functional (e.g., the HF exchange only functional) is used in the calculations.
[47]Z. R. Grabowski, K. Rotkiewicz, W. Rubaszewska, and E. Kirkor-Kaminska, Acta Phys. Polon. **A54**, 767 (1978).
[48]W. Rettig and B. Zietz, Chem. Phys. Lett. **317**, 187 (2000).
[49]B. Mennucci, A. Toniolo, and J. Tomasi, J. Am. Chem. Soc. **122**, 10621 (2000).
[50]C. Jamorski, J. B. Foresman, C. Thilgen, and H.-P. Lüthi, J. Chem. Phys. **116**, 8761 (2002).
[51]A. Köhn and C. Hättig, J. Am. Chem. Soc. **126**, 7399 (2004).
[52]A. D. Becke, Phys. Rev. A **38**, 3098 (1988); C. Lee, W. Yang, and R. G. Parr, Phys. Rev. B **37**, 785 (1988).
[53]P. J. Stevens, F. J. Devlin, C. F. Chablowski, and M. J. Frisch, J. Phys. Chem. **98**, 11623 (1994).
[54]A. D. Becke, J. Chem. Phys. **98**, 1372 (1993).
[55]C. Bulliard, M. Allan, G. Wirtz, E. Haselbach, K. A. Zachariasse, N. Detzer, and S. Grimme, J. Phys. Chem. A **103**, 7766 (1999).
[56]O. Christiansen, H. Koch, and P. Jørgensen, Chem. Phys. Lett. **243**, 409 (1995); C. Hättig and F. Weigend, J. Chem. Phys. **113**, 5154 (2000).
[57]M. Krykunov and T. Ziegler, J. Chem. Theory Comput. **9**, 2761 (2013).
[58]M. Krykunov, M. Seth, and T. Ziegler, J. Chem. Phys. **140**, 18A502 (2014).
[59]P. E. Hartnett, A. Timalsina, H. S. S. R. Matte, N. Zhou, X. Guo, W. Zhao, A. Facchetti, R. P. H. Chang, M. C. Hersam, M. R. Wasielewski, and T. J. Marks, J. Am. Chem. Soc. **136**, 16345 (2014).
[60]J. Vura-Weis, M. A. Ratner, and M. R. Wasielewski, J. Am. Chem. Soc. **132**, 1738 (2010); C. Xue, Q. Dong-Dong, Z. Yue-Xing, B. Yong-Zhong, and J. Jian-Zhuang, Acta Phys.-Chim. Sin. **26**, 1059 (2010); J. Wenzel, A. Dreuw, and I. Burghardt, Phys. Chem. Chem. Phys. **15**, 11704 (2013).
[61]A. Schäfer, H. Horn, and R. Ahlrichs, J. Chem. Phys. **97**, 2571 (1992).
[62]J.-D. Chai and M. Head-Gordon, Phys. Chem. Chem. Phys. **10**, 6615 (2008).
[63]For the CC2/cc-pVDZ calculation, the $\%\mathcal{T}_2$ criteria amount to 9.80% (S_1) and 8.08% (S_2), which indicates that the obtained CC2 excitation energies should be reliable. The D_1 diagnostics of the multi-reference character of the ground state, $D_1 = 0.0842$, suggest that the S_0 state is mildly multi-reference. According to general experience, the CC2 results remain sufficiently reliable for D_1 in the range <0.10–0.15. [A. Köhn and C. Hättig, J. Chem. Phys. **119**, 5021 (2003)].